

CHAPTER 5

Growth and Characterization of Intrinsic Zinc Oxide (i-ZnO) and Aluminum doped Zinc Oxide (AZO) – as a Window Layer

5. Growth and Characterization of Intrinsic Zinc Oxide (i-ZnO) and Aluminum doped Zinc Oxide (AZO) – as a Window Layer

The window layer in copper indium diselenide (CIS) based thin film solar cell is used to collect and transport the photocurrent produced at the junction and, at the same time, allow the largest possible number of photons to reach the junction itself. These are mutually dependent properties of materials and only in transparent conductive oxides (TCO), as aluminum doped zinc oxide (ZnO:Al) these properties are both enhanced to a reasonable level of performance at reasonable costs. In this study, we have prepared undoped zinc oxide (i-ZnO) target having diameter of ~50 mm using the method of grouting and sintering from 99.9 % pure ZnO powder obtained from Sigma Aldrich (U.S.A.). Structural property of the prepared target is investigated. The window layer used within this work is made by a double layer composed of a thin (70 nm) undoped zinc oxide layer, often referred to as i-ZnO, and a thicker (600 nm) aluminum doped zinc oxide (AZO) layer with 2 wt % content of Al₂O₃. Thin films of i-ZnO and AZO are deposited using RF magnetron sputtering technique. The properties of ZnO as TCO for CIS based thin film solar cell device and the structural, optical and electrical properties of i-ZnO and AZO thin films are elaborated in this chapter.

5.1 Transparent Conductive Oxide (TCO) in CIS Thin Film Solar Cells

Transparent conductive oxide (TCO) used in CIS based thin film solar cells is a double layer composed of a thin (70 nm) undoped zinc oxide layer (i-ZnO), and a thicker (600 nm) aluminum doped zinc oxide (ZnO:Al or AZO). ZnO thin films can be deposited by a variety of deposition techniques such as radio frequency magnetron sputtering [138], direct current magnetron sputtering [139], and metal organic chemical vapor phase deposition [140]. The material properties (i.e. structural, optical and electrical properties) of the ZnO thin film is critically related to the specific growth technique employed and to the growth parameters used. In this study, we have used RF magnetron sputtering technique to deposit i-ZnO and

AZO thin films. The role of these layers in CIS based thin film solar cells can be summarized as:

- Contribute to the formation of the heterojunction
- The lateral transport of the photocurrent with the lowest possible ohmic losses.
- The transmission of light to the absorber.

A deeper insight into these three points with general properties of ZnO is detailed here.

5.1.1 Heterojunction Formation

The first CIS based thin film solar cell was based upon the heterojunction between CIS and a relatively thick layer of CdS. Although it shows a good band alignment (figure 5.1) with CIS and a good matching of lattice parameters, some disadvantages lead to the choice of extremely reducing the thickness of the CdS layer down to about 50 nm. These disadvantages concern the low conductivity due to the low carrier density [141] of about 10^{16} cm^{-3} and to the strong absorption of light below 517 nm due to its bandgap of about 2.4 eV.

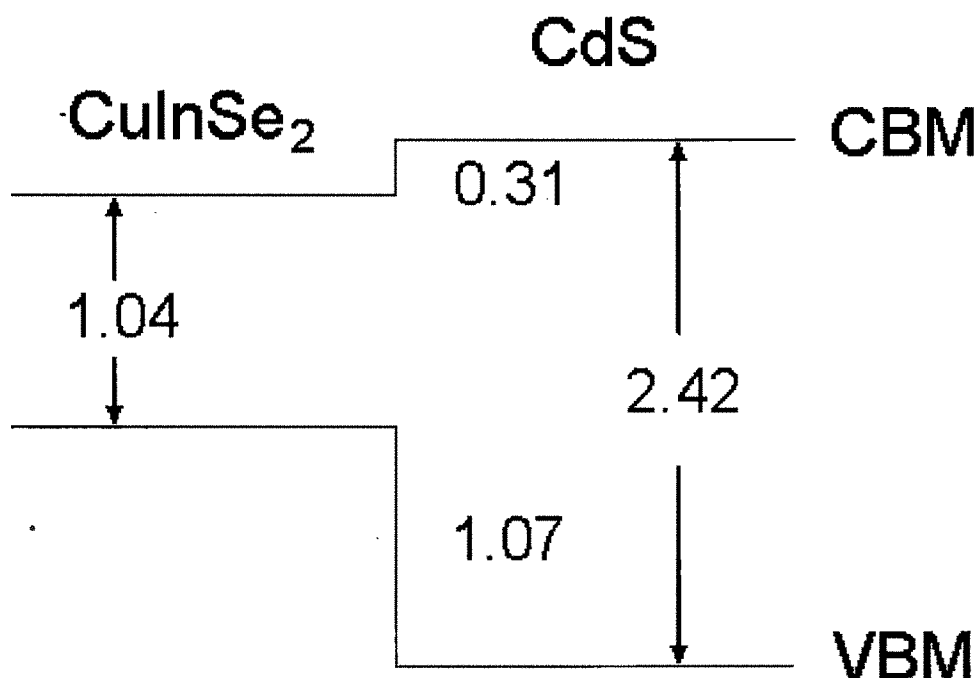


Figure 5.1: Band offsets in the heterojunction formation between CIS and CdS.

Therefore, doped and wide bandgap semiconductor as a window layer in CIS based thin film solar cell device has been introduced. Nonetheless, the reduced thickness of the buffer layer causes the window layer, to be involved in the heterojunction formation, which directly affects the electronic properties at the CIS/CdS interface.

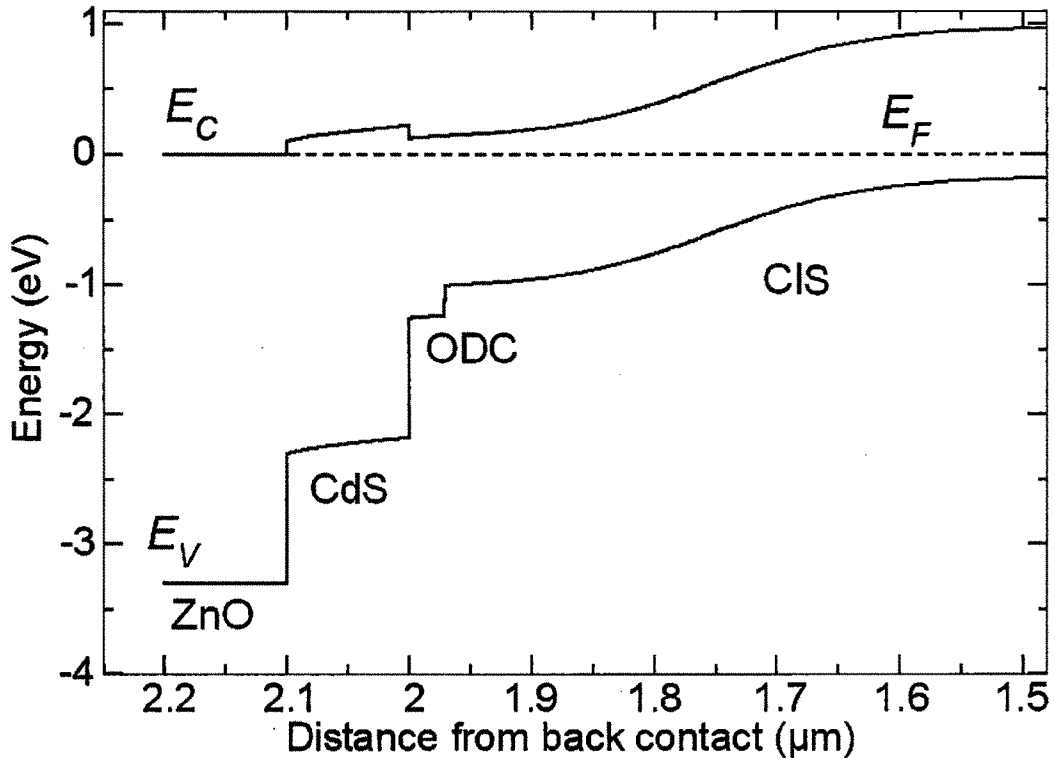


Figure 5.2: Electronic band diagram of the buried junction occurring in a suitably doped CIS/CdS/ZnO solar cell.

In order to realize an efficient device, the Fermi level in the absorber layer at the interface with the buffer layer should be [142] as close as possible to the conduction band. This produces a so-called buried junction (figure 5.2) that causes the surface region of the absorber to be inverted to an n-type region. This also means that the actual junction is located inside the absorber layer thus reducing the interface recombination, also in presence of high recombination velocities, because of a limited concentration of holes. Further advantages could come from the formation of an ordered defect compound (ODC) layer at the surface of the CIS or by adjusting the bandgap of the absorber to higher values or creating a gradient in the bandgap profile [143].

5.1.2 Lateral Transport of Charge

The main function of AZO layer is the collection and transport of the produced photocurrent from the heterojunction to the negative contact of cells and modules. In small lab-scale cells, an additional aluminum grid is deposited on the AZO layer to improve collection.

The conduction mechanism in cell is based upon both intrinsic defects and intentionally introduced defects, typically Al ions. For what concerns the former kind of

defect, was found [144] that ZnO is n-type at Zn-rich conditions. This is because the Zn interstitial (Zn_i), is a shallow donor, supplying electrons and its formation enthalpy is low for both Zn-rich and O-rich conditions, so this defect is abundant. Moreover the native defects that could compensate the n-type doping effect of Zn_i , O, O_i , and Zn vacancy, V_{Zn} have high formation enthalpies for Zn-rich conditions, so these “electron killers” are not abundant. However, in O-rich conditions, the equilibrium is moved in favor of O_i and V_{Zn} , thus drastically reducing the free carrier’s densities and leading to very high resistivity ($\sim 10^9 \Omega \text{ cm}$) of the un-doped material. The extrinsic doping, typically obtained by adding a 2 wt. % [145] of Al_2O_3 , causes the formation of substitutional aluminum defects (Al_{Zn}) in ZnO crystal structure having the transition donor/neutral level at $E_c-0.012 \text{ eV}$ [144], where E_c is the energy level at the bottom of the conduction band of ZnO.

High resistive i-ZnO, between buffer and window layer in CIS thin film solar cell device could appear to be unfavorable and requires additional industrial cost. However, for large area modules such layer is used to prevent major losses due to unintentional shunt paths and, may be to a higher degree of importance, to limit the efficiency losses due to inhomogeneities of the electronic characteristics of large area [146].

5.1.3 Photon Transmission to the Absorber

On the run to the best efficiency, every more photon that is able to reach the junction is important. Thus, the optical properties of the window layer results to be of particular interest in the optimization of solar cells. ZnO with direct bandgap energy of 3.37 eV [147] would appear to be an ideal material for this purpose having a high transparency in the absorption wavelength range of CIS cells and additionally having a low cost. The actual value of the bandgap energy E_g depends upon the occupation of the conduction band showing a blue shift ΔE_g known as the Moss-Burnstein effect [148] and expressed as:

$$E_g = E_g^0 + \Delta E_g \quad (5.1)$$

where E_g^0 is the energy gap for the intrinsic ZnO.

Assuming a spherical Fermi surface, the blue shift in the energy bandgap can be calculated [149] by using the free electron concentration n_e according to:

$$\Delta E_g = \frac{h^2}{8m_e^*} \left(\frac{3n_e}{\pi} \right)^{2/3} \quad (5.2)$$

The use of thin layers implies the occurring of the optical phenomenon of interference that results in oscillations in the intensity of transmission spectra as shown in figure 5.3. This

can be controlled with the use of antireflection coatings or with careful optical design of stacked film structures.

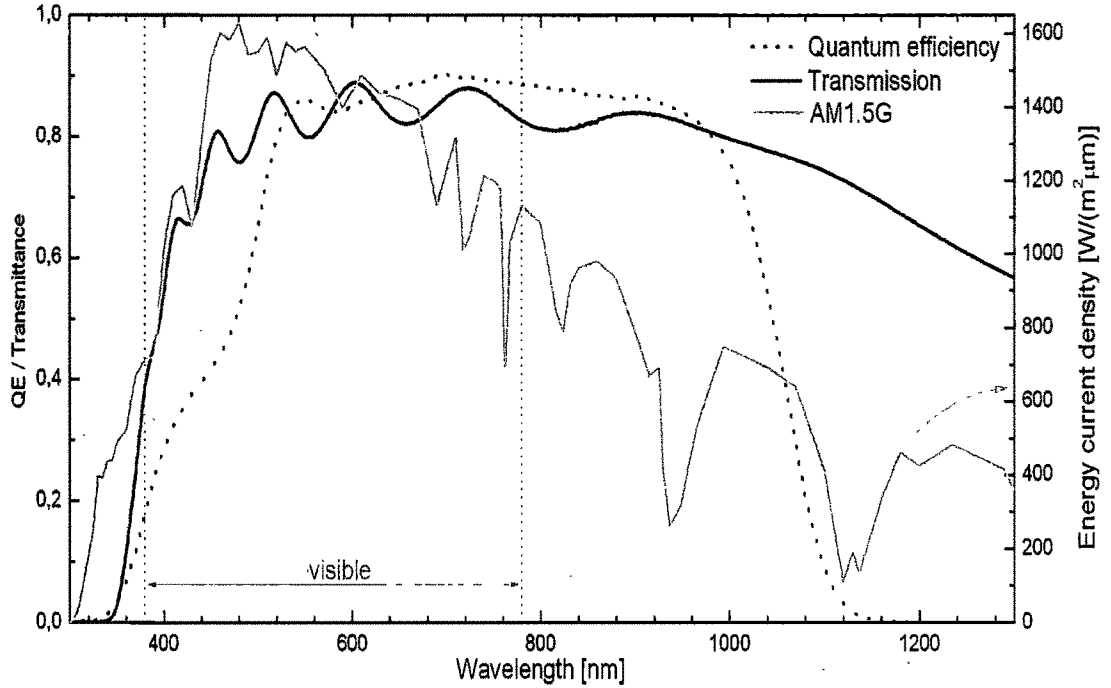


Figure 5.3: Comparison between the transmission spectrum of a typical 790 nm thick AZO layer on glass (black solid line), a quantum efficiency spectrum for a typical CIS solar cell (dotted line, active area efficiency) and the AM1.5 standard solar spectrum (solid light gray line).

The refractive index of AZO thin film can be calculated [150] by using the Cauchy's equation

$$n(\lambda) = n(\infty) + \frac{B}{\lambda^2} + \frac{C}{\lambda^4} \quad (5.3)$$

Here the parameter $n(\infty)$ depends upon the doping of ZnO layer varying from about 1.85 for the i-ZnO layer to about 1.78 for AZO layer. Here B and C are fitting parameters determined by fitting the transmission curve with AM1.5 standard solar spectrum curve.

5.1.4 Crystal Structure and Physical Properties of Zinc oxide

Zinc oxide (ZnO) crystallizes in two different crystal lattices. The first is the hexagonal wurtzite lattice, which is mainly used in the thin film industry as a transparent conducting oxide or as a catalyst in methanol synthesis [151]. The second structure is more known to the geologist as the rocksalt structure (at high pressure). This structure is a spinal phase that is used in the understanding of the Earth's lower mantle [152]. The crystallographic structure is important in determining the orientation of thin films of ZnO. The hexagonal wurtzite crystal lattice of single crystal ZnO is depicted in figure 5.4. The unit cell contains two zinc (Zn) cations and two oxygen (O) anions. The ZnO crystal thus can be viewed as a sequence of O-Zn double layers stacked along the c-axis direction (figure 5.4). This structure is well known to show piezoelectric properties with a large electromechanical coupling factor and a low dielectric constant [153]. Table 5.1 summarizes the most significant properties of ZnO.

Table 5.1: Physical properties of ZnO single crystal. [154]

Crystal System	Wurtzite
Lattice System	a = 0.3253 nm, c = 0.5211 nm
Sublimation point	2248 ± 25 K
Optical transparency	0.4 - 2.5 μm
Refractive index	$n_0 = 1.9985, n_c = 2.0147 (\lambda = 6328 \text{ \AA})$

5.2 Method of Preparing i-ZnO Target

High-quality sputtering targets are important in obtaining superior thin film properties. Transparent conducting oxide thin film targets can be divided into two types - metal targets and powder oxide-sintering targets. If metal targets are adopted, then oxygen gas must be first introduced into the chamber to form a thin-film oxide through chemical reactions. However, this method does not easily yield stable quality deposited film. Therefore, a powder oxide-sintering target is preferred [155]. Three conventional methods, using a hot press, a hot isostatic press and normal sintering, exist for making powder oxide sintering targets. Large-scale targets are more easily produced by normal sintering process. This work adopted the methods of grouting and normal sintering to produce good quality sputtered targets.

ZnO powder (99.99 %) obtained from Sigma-Aldrich (U.S.A.) is used to prepare i-ZnO target. ZnO powder is dry-pressed or palletized by applying force of 5 ton for three minutes in 51 mm diameter stainless steel die using droplets of acetone as binding material. The resultant disc shaped pellet (target) has 50 mm (± 1 mm) diameter.

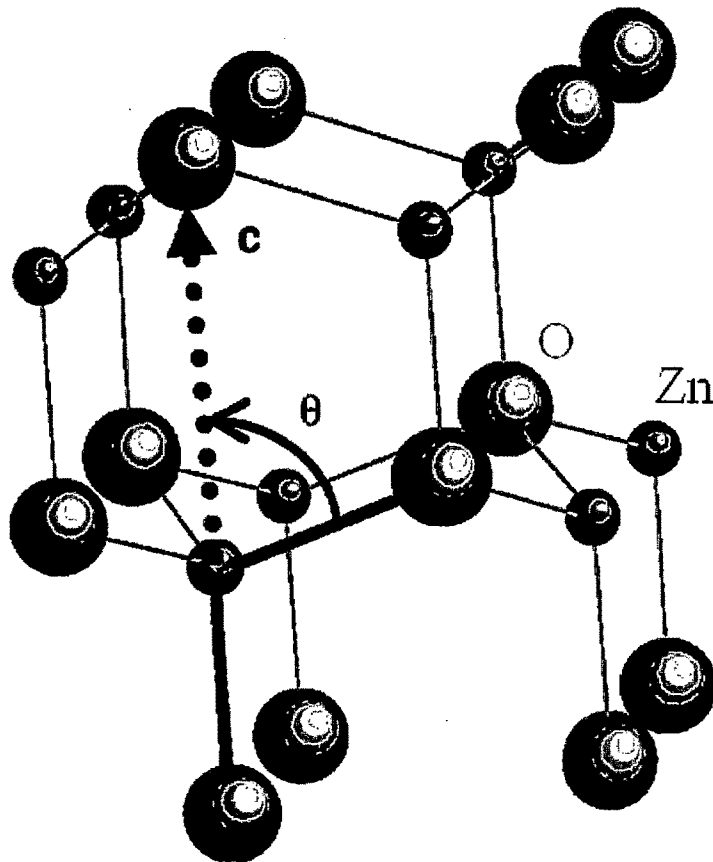


Figure 5.4: The wurtzite lattice of zinc oxide: small circles represent the zinc atoms, while large circles depict oxygen atoms [156].

5.2.1 Sintering of i-ZnO Target

The target is first sintered at 673 K temperature in an electric furnace at atmospheric pressure. The heating rate of furnace is kept at 5 K per minute. The target is maintained at elevated temperature for six hour after which the temperature of the furnace is allowed to cool down to the laboratory temperature at the same rate. The shrinkage of the target is developed. Therefore, the target is crushed to powder using pestal and mortar. The sintered powdered material is then used to prepare the pellet (target) again. The target is sintered at 1423 K for twenty-four hours. Figure 5.5 shows as prepared target of i-ZnO having diameter of 50 mm (± 1 mm).



Figure 5.5: i-ZnO target having diameter of 50 mm (\pm 1 mm) prepared using method of grouting and sintering.

5.2.2 Structural Characterization of i-ZnO Target

The crystalline structure of i-ZnO target is investigated by X-ray diffraction (XRD) analysis in 2θ range from 20° to 100° . Figure 5.6 shows the XRD pattern of i-ZnO target. All major peaks for Zinc Oxide are identified in XRD and correspond well with JCPDS data card (file No. 36-1451).

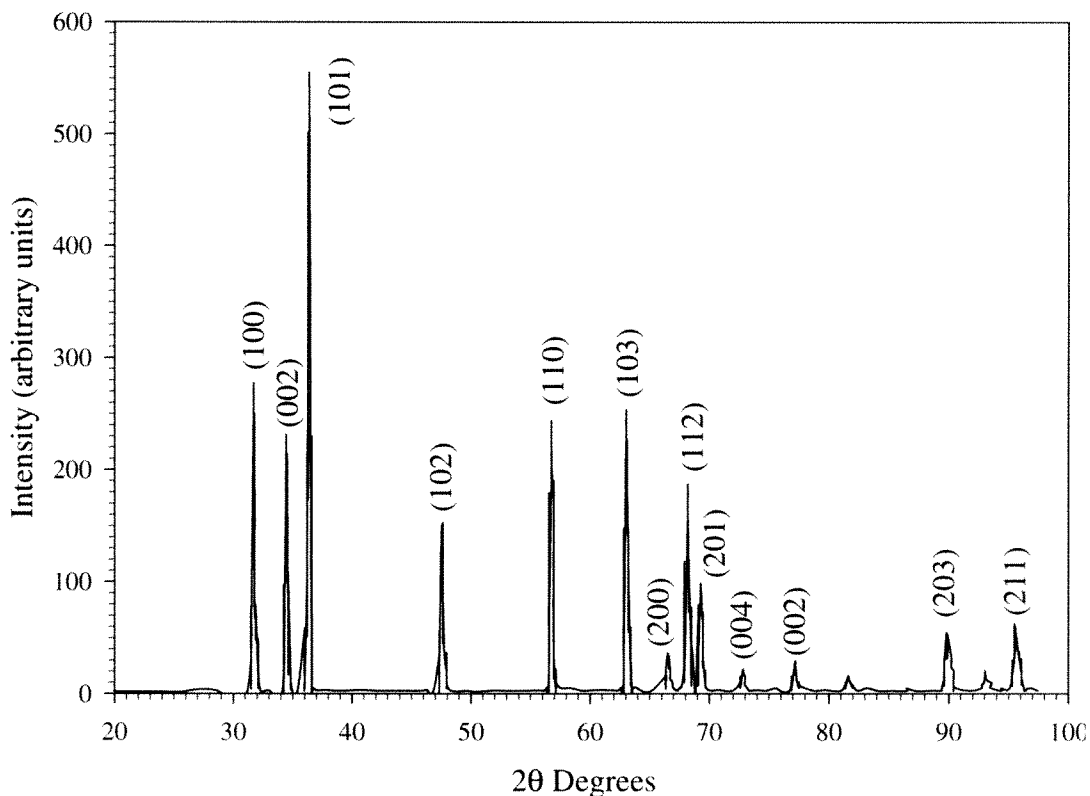


Figure 5.6: XRD spectrum of i-ZnO target.

5.3 RF Magnetron Sputtering of i-ZnO Thin Films

The front contact of CIS based thin film solar cell consists of a highly conductive ZnO:Al layer on top of a highly resistive layer of intrinsic ZnO (i-ZnO). The very thin high resistive layer of i-ZnO prevents a shunt path between the molybdenum back contact and the aluminum doped zinc oxide front contact. For CIS based solar cell device application thickness of i-ZnO layer and its' resistivity are important parameters. The correlation of the cell performance of CIS based solar cells with the thickness of highly resistive i-ZnO layer is studied in detail by Ishizuka et al. [157]. Their study reveals that the efficiency of CIS based thin film solar cell depends on the i-ZnO thickness, and the highest efficiency is achieved when the thickness of the i-ZnO layer is about 70 nm. In the case where i-ZnO layers are thinner than 40 nm, a slight degradation in cell performance was observed and cell efficiency reproducibility worsened. On the contrary, when i-ZnO layers were thicker than 70 nm, cell efficiency again degraded. In this study, we have deposited i-ZnO thin film of 70 nm thickness from prepared target initially on glass substrates using deposition parameters listed in Table 5.2.

Table 5.2: RF magnetron sputtering condition for i-ZnO thin film deposition.

Target Substrate distance	50 mm
Sputtering temperature	Room temperature
Sputtering gas	Argon
RF power	100 W
Deposition pressure	1 mTorr

The resistivity of i-ZnO thin film prepared under the conditions listed in table 5.2 is 4.7×10^5 G Ω cm. The value of resistivity is close to the reported value for CIS solar cell application by researchers [120,157]. The structural, morphological, optical and electrical property of i-ZnO thin film is investigated.

5.4 Characterization of i-ZnO Thin Films

The structural characterization of i-ZnO thin film prepared using RF magnetron sputtering technique is carried out using an X-ray diffractometer (Shimadzu Lab X 6000). The surface morphology of i-ZnO thin film is studied using AFM technique. The optical transmittance measurements are carried out in the wavelength range 320 nm-900 nm using the monochromator CM 110, photo detector 816-SL type (Newport) and lock-in amplifier SR-530.

5.4.1 Structural Characterization

The crystalline structure and orientation of the i-ZnO thin film is investigated by X-ray diffraction (XRD) analysis, in 2θ range 20° - 80° at a scan rate $0.05^\circ \text{ s}^{-1}$ with Cu K_α ($\lambda = 0.154$ nm) radiation source. Figure 5.7 shows the XRD pattern of i- ZnO thin film deposited using the parameters listed in table 5.2. Major peak is observed at diffraction angle $2\theta = 34.421^\circ$. This diffraction angle corresponds to (002) plane of reflections. JCPDS data card (file 36-1451) reveals that the film has strong c-axis orientation and hexagonal structure.

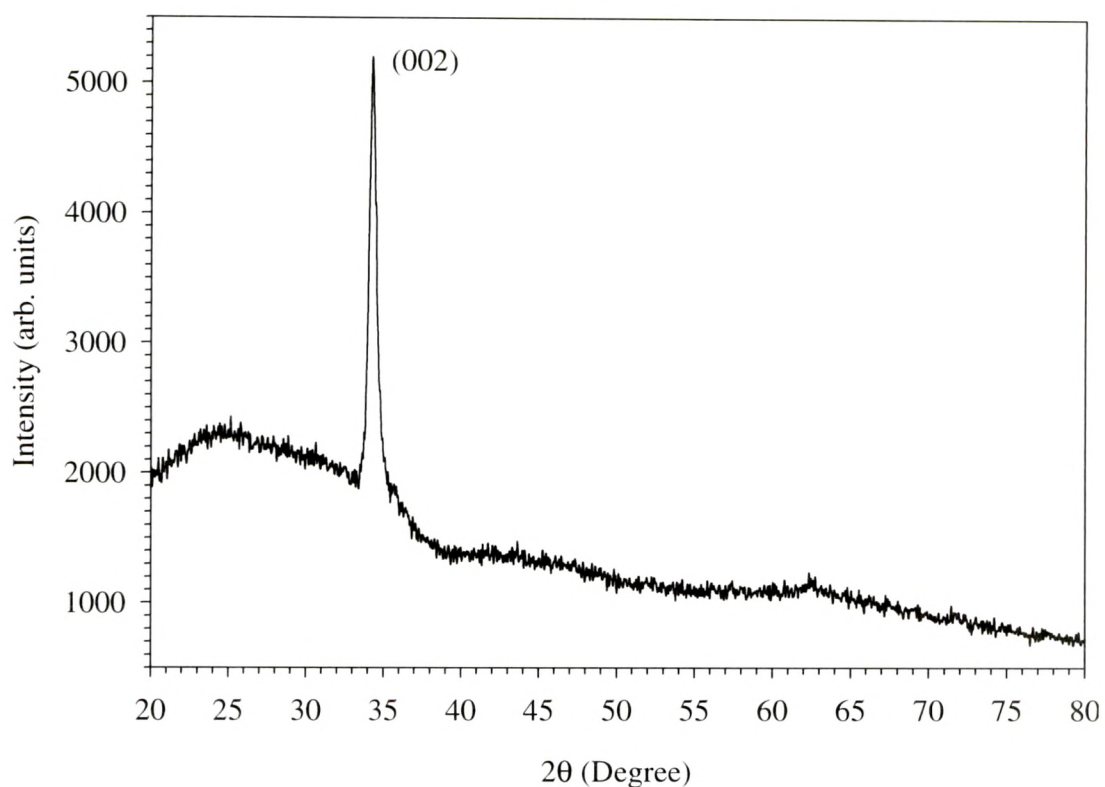


Figure 5.7: X-Ray diffraction pattern of i-ZnO thin film.

5.4.2 Morphological Characterization

The morphological characteristic of i-ZnO thin film is studied using atomic force microscope. Figure 5.8 shows two and three-dimensional AFM images of i-ZnO thin film.

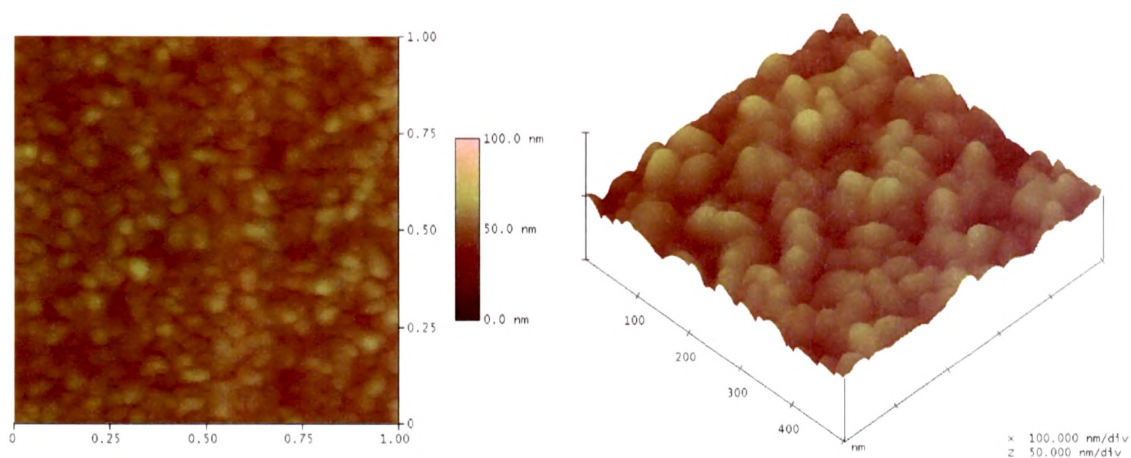
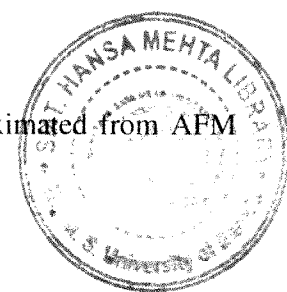


Figure 5.8: AFM image of i-ZnO thin film.

AFM image of the film reveals a structure with dense grains. The irregular shape of the grains suggests that the kinetic energy of molecules reaching the substrate is not sufficient for



the coalescence of the grains. The surface roughness of the film approximated from AFM analysis is 4 nm.

5.4.3 Optical Characterization

Figure 5.9 depicts transmission spectrum of i-ZnO layer. In order to obtain highly resistive i-ZnO layer deposition is carried out at higher deposition pressure. It is seen that i-ZnO layer exhibited very high transmission (above 85 %) in the visible range.

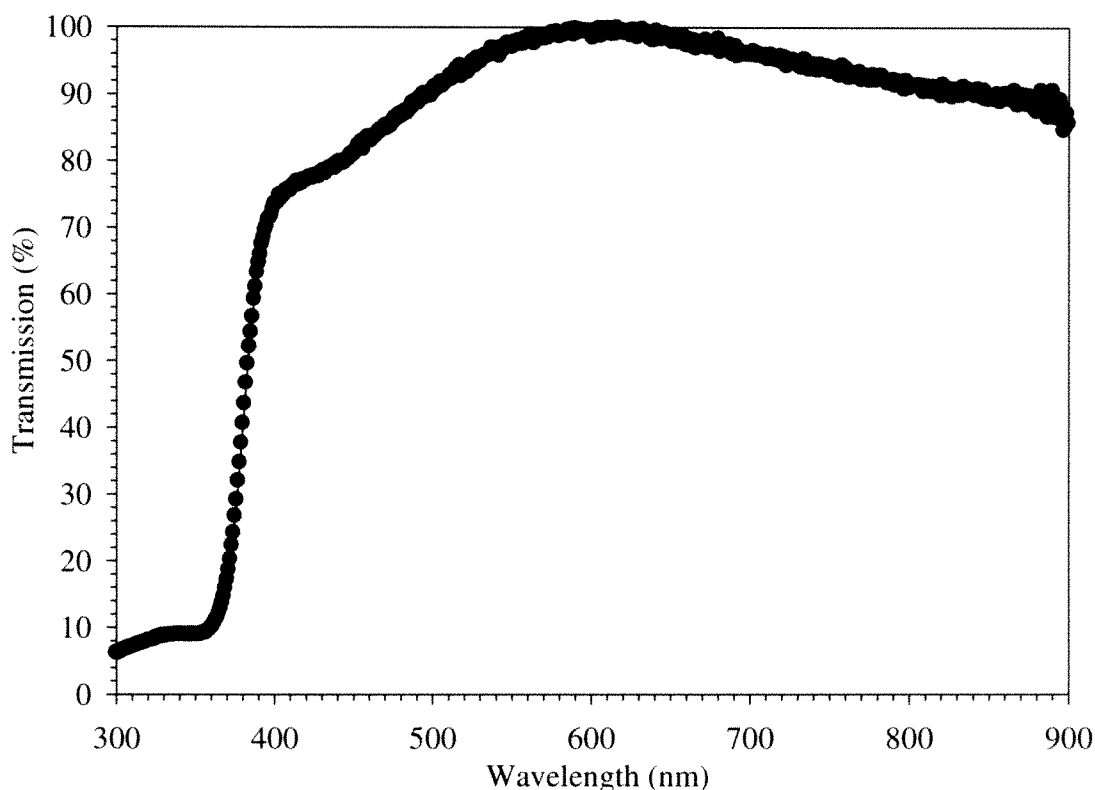


Figure 5.9: Transmission spectrum of i-ZnO thin film.

The optical bandgap of the film is calculated using plot of $(\alpha h\nu)^2$ versus $h\nu$ (shown in figure 5.10). The value of energy bandgap for i-ZnO thin film can be estimated by extrapolating the linear portion of the absorption edge with energy axis to find the intercept. Energy bandgap of i-ZnO thin film using the linear fit is 3.25 eV. It is in good agreement with the reported value by researchers using different deposition techniques [158,159,160].

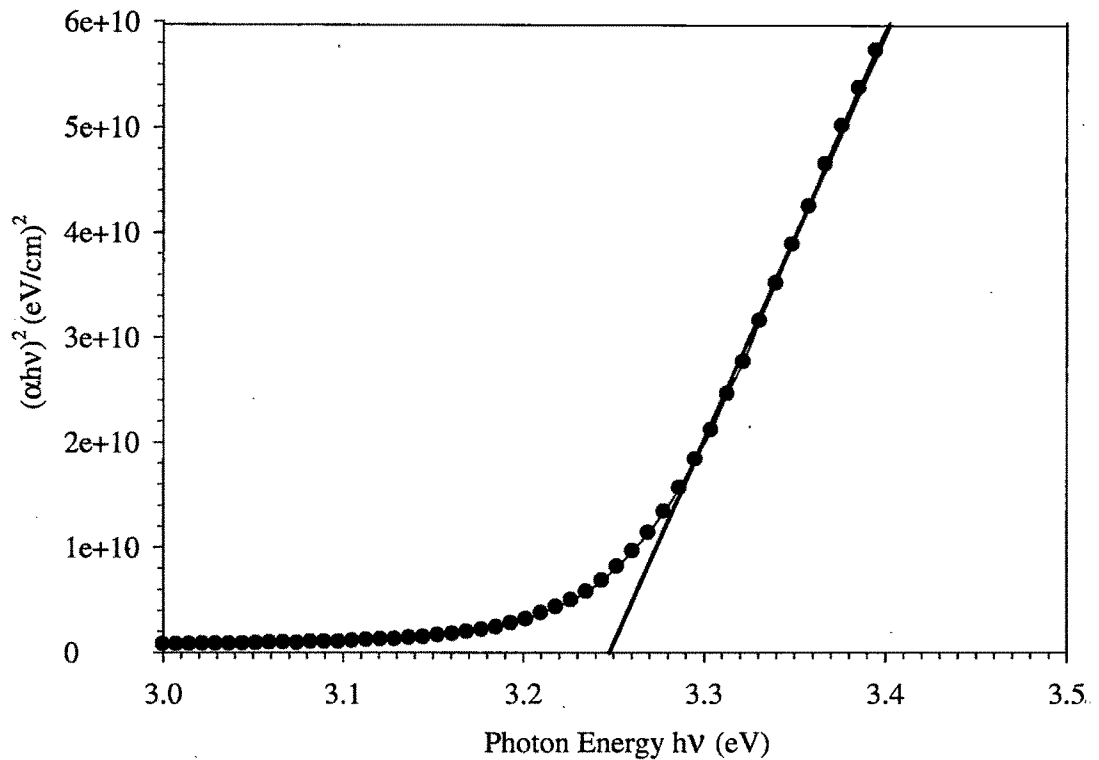


Figure 5.10: Variation of $(\alpha h\nu)^2$ versus $h\nu$ of i-ZnO thin film.

5.5 AZO Target Characterization

The ceramic AZO (2 wt % Al_2O_3 doped), 99.9 % pure, target shown in figure 5.11, manufactured by GmbH Germany is used as sputtering target to deposit AZO thin films. The AZO target is characterized by XRD before using it for sputtering process.

5.5.1 Structural Characterization of AZO Target

The XRD spectrum of the AZO target is shown in figure 5.12. Through identifications of XRD spectrum suggests that all peaks presented in the spectra are from the ZnO crystal structure [161].

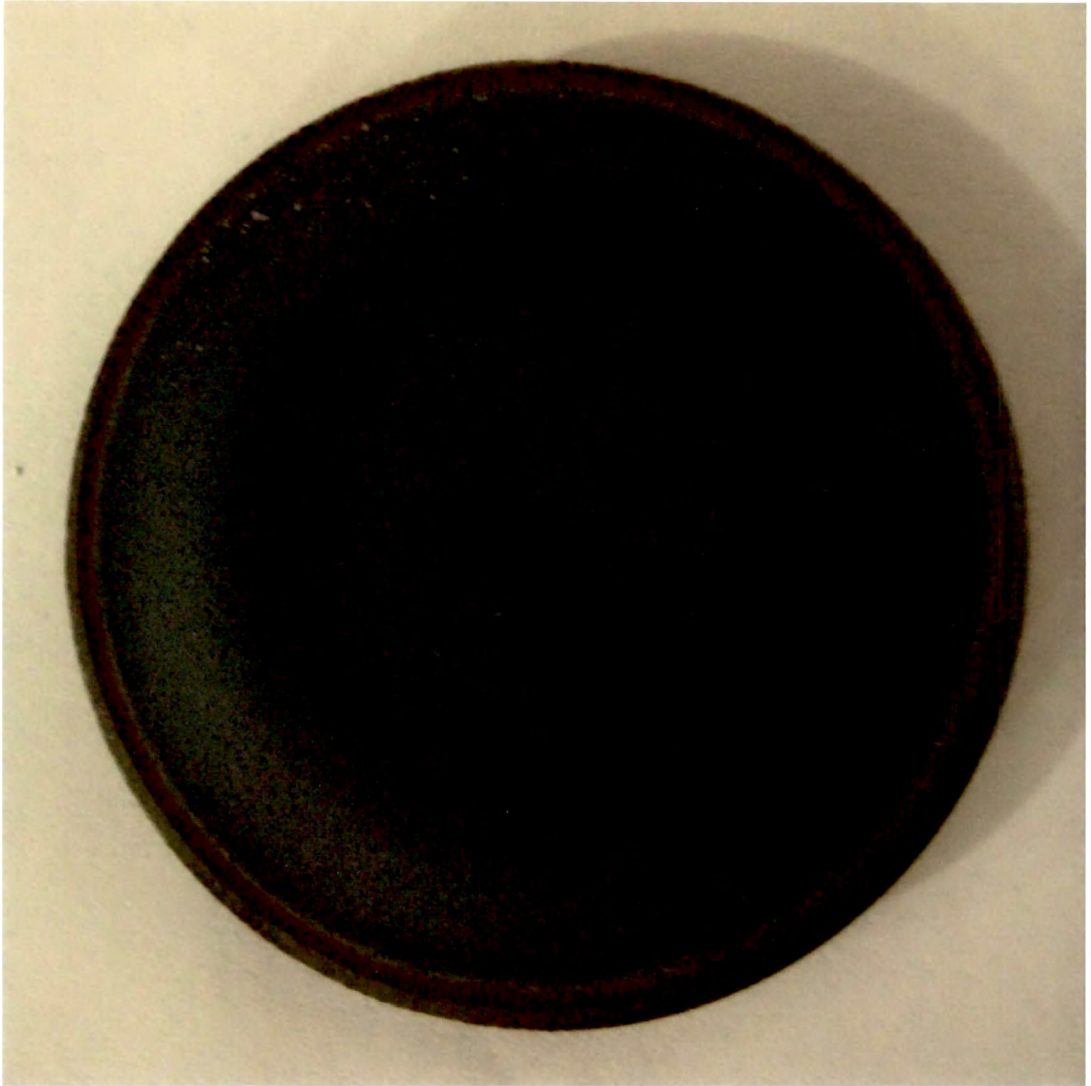


Figure 5.11: AZO (2 wt % Al₂O₃ doped ZnO) target having diameter of 50 mm (± 1 mm).

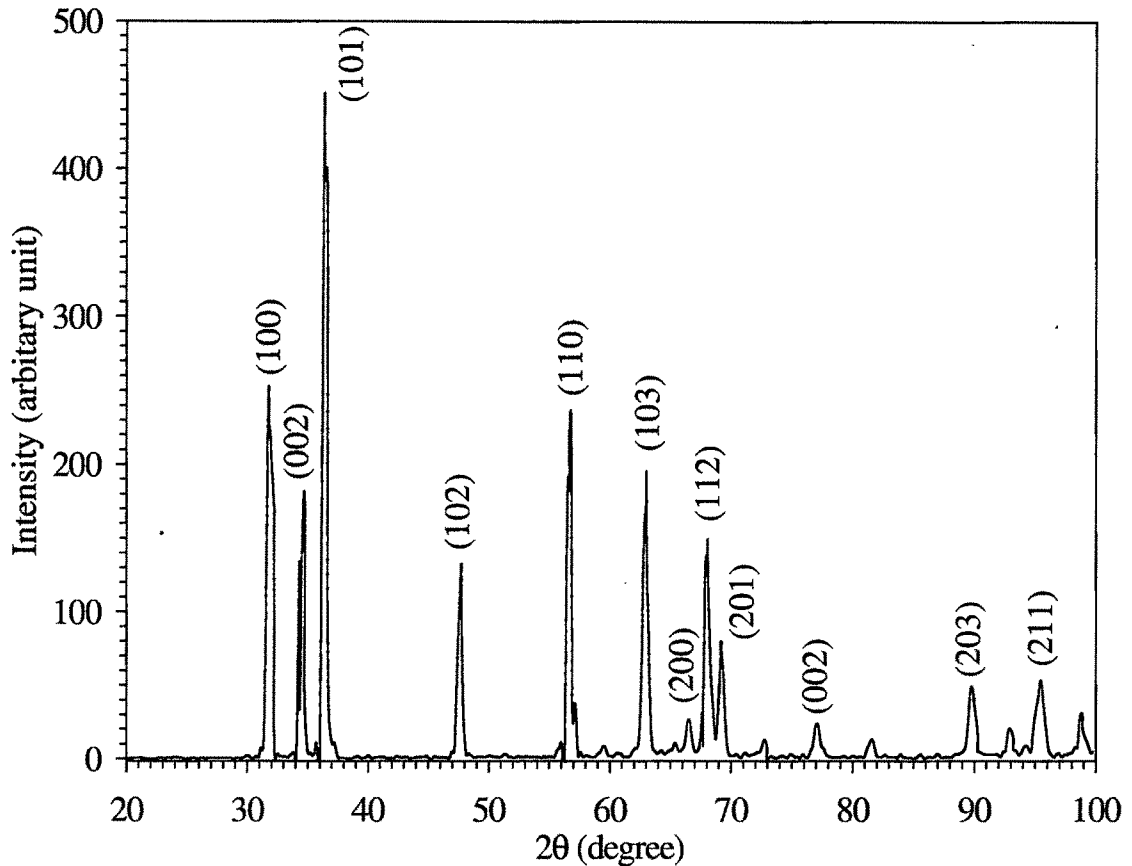


Figure 5.12: The XRD spectra of the AZO target

5.6 RF Magnetron Sputtering of AZO Thin Films

Aluminum doped zinc oxide (AZO) transparent conductive oxide films have high transmittance in the visible region and low resistivity. In our work, the deposition parameters for AZO films are first optimized on 2 mm thick soda lime glass substrates using RF-magnetron sputtering technique.

The depositions are carried out in pure argon ambient keeping the target-substrate constant at 50 mm. The thicknesses of the as-deposited AZO films are approximated in-situ using quartz crystal microbalance. To optimize deposition parameters we have deposited AZO thin films by varying deposition pressure, keeping RF power constant (100 W). The structural, morphological, optical and electrical properties of the AZO thin films deposited are investigated.

5.6.1 Study as a Function of Working Pressure

We have investigated the effect of the working pressure, on the different properties of the AZO thin films deposited in the working pressure range of 2 to 20 mTorr keeping RF power constant at 100 W. It is observed during film deposition that the deposition rate varies significantly with the working pressure. In our case the deposition rate is higher (0.32 nm/s) for lower pressure (2 mTorr) and lower (0.15 nm/s) for higher pressure (20 mTorr). This is the key factor, which affect the properties of the thin films.

5.6.1.1 Structural Characterization

The XRD spectra of AZO thin film deposited at different working pressure (2 to 20 mTorr) keeping RF power constant at 100 W is shown in figure 5.13. It indicates that on increasing the working pressure from 2 mTorr to 10 mTorr, the intensity of the (002) peak increases up to 10 mTorr working pressure and by further increment in the working pressure i.e. at 20 mTorr the intensity of (002) peak decreases significantly. The improvement in the intensity of (002) peak shows improvement in the crystallinity of the film. The crystallite size calculated from the Scherrer's formula is 8 nm for 2 mTorr working pressure and it is increased as the pressure increases and reaches the maximum value of 10 nm. The variation in the crystallite size, FWHM, d-value and its corresponding 2θ value is shown in table 5.3. The improvement in the crystalline quality of the films and the crystallite size show the enchantment in the possibility of Al doping in ZnO.

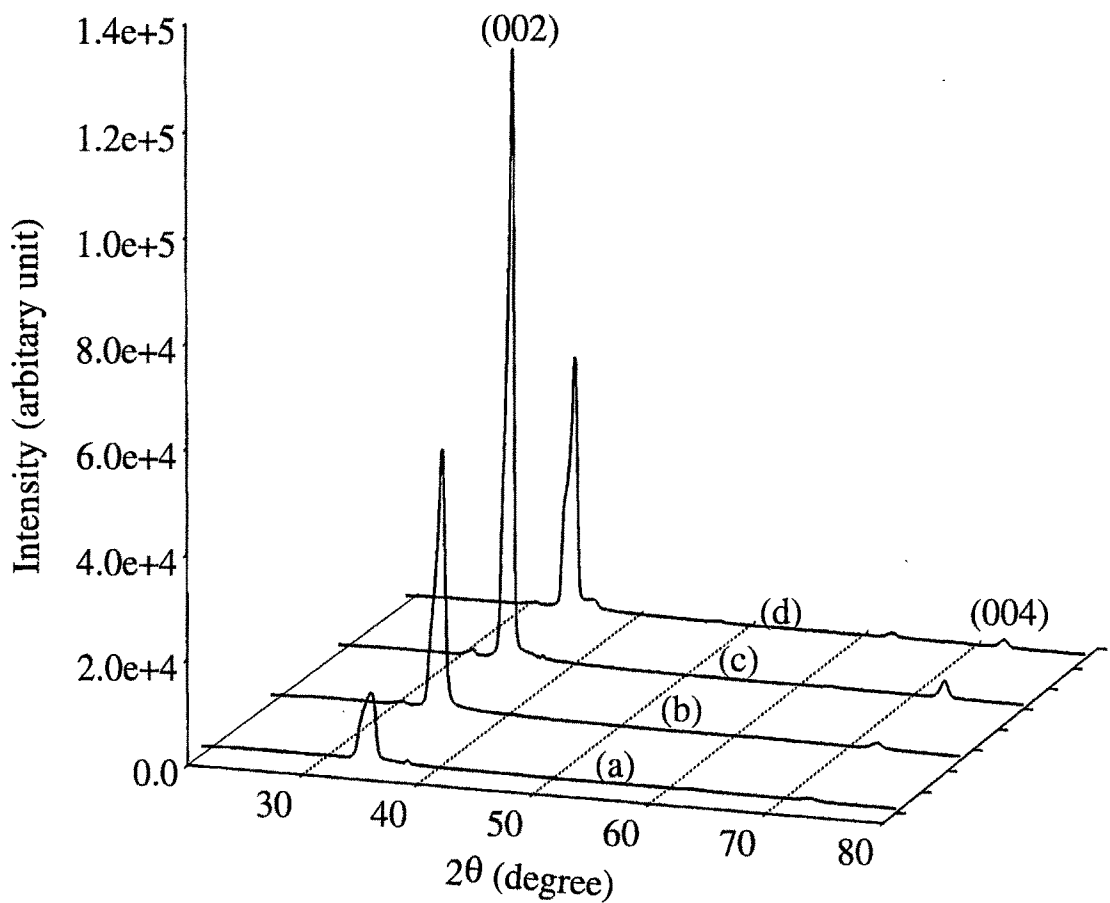


Fig. 5.13 The XRD spectra of the AZO thin films deposited at (a) 2 mTorr, (b) 5 mTorr, (c) 10 mTorr.

Table 5.3: The d-spacing, FWHM, and the crystallite size of the AZO thin films grown at different working pressure by keeping RF power constant at 100 W.

Working pressure (mTorr)	d-spacing (Å)	FWHM (degree)	Crystallite size d (nm)
2	2.56	0.99	8
5	2.55	0.96	9
10	2.55	0.85	10
20	2.557	1.000	8

5.6.1.2 Morphological Characterization

Figure 5.14 shows the AFM image of the AZO thin films grown at different working pressures keeping RF power constant at 100 W. It is observed that the morphology of the films strongly depends on the working pressure. The grain growth depends on deposition flux reaching the substrate, which is higher at lower working pressure as there is less scattering

probability of the sputtered and gas atoms. This results in non-uniform growth of grains at 2 mTorr working pressure.

As we move from 2 mTorr to 20 mTorr, there is a decrease in energetic particle bombardment. This is responsible for the uniform grain formation. The increased surface roughness from 19 nm to 26 nm, by increasing the working pressure from 2 mTorr to 10 mTorr is likely an indicator of increased grain size, consistent with the XRD data.

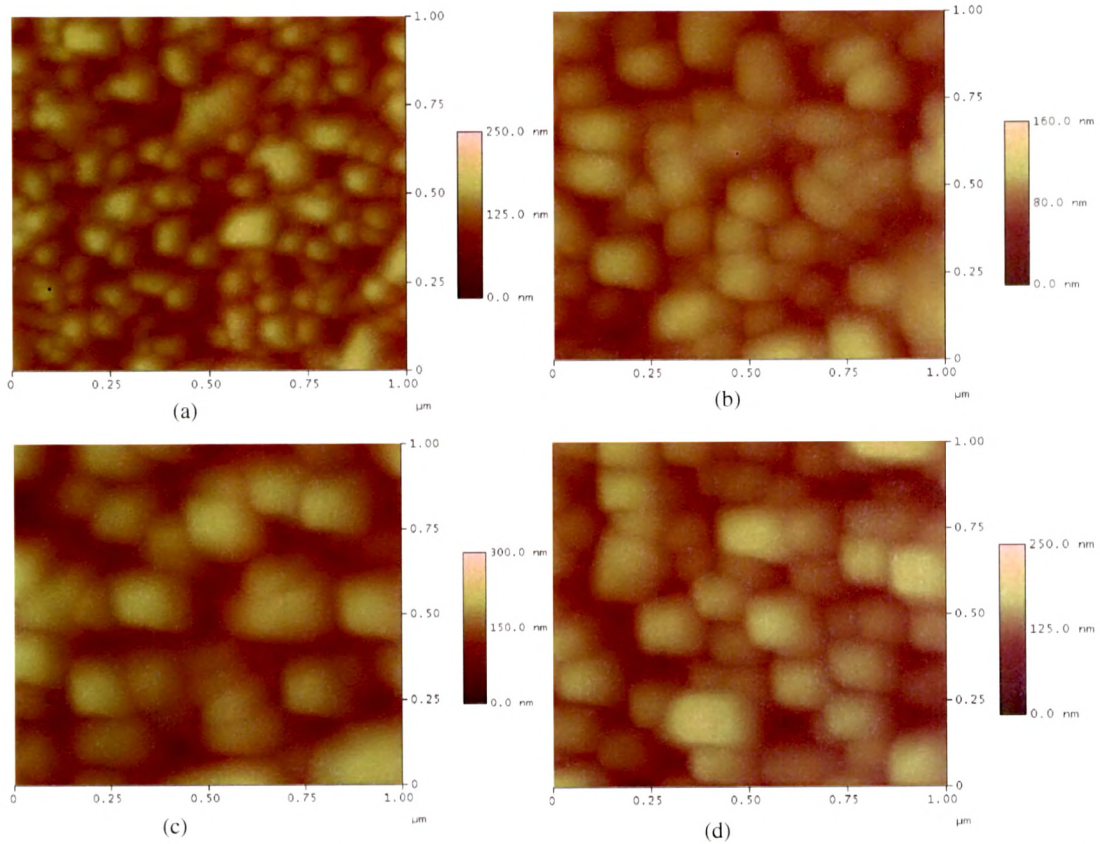


Figure 5.14: The AFM images of the AZO thin films deposited at (a) 2 mTorr, (b) 5 mTorr, (c) 10 mTorr, (d) 20 mTorr working pressures.

5.6.1.3 Optical Characterization

The optical transmission spectrum of AZO thin films grown at different working pressures is shown in figure 5.15. As the working pressure changes from 2 mTorr to 20 mTorr variation in transmission with wavelength is observed. The value of energy bandgap estimated for films deposited at different working pressure viz. 2 mTorr to 20 mTorr is in the range of 3.38 eV to 3.31 eV, which is shown in figure 5.16. Decrease in energy bandgap with increase in

working pressure can be explained by examining the dependence of the Al inclusion as a function of working pressure.

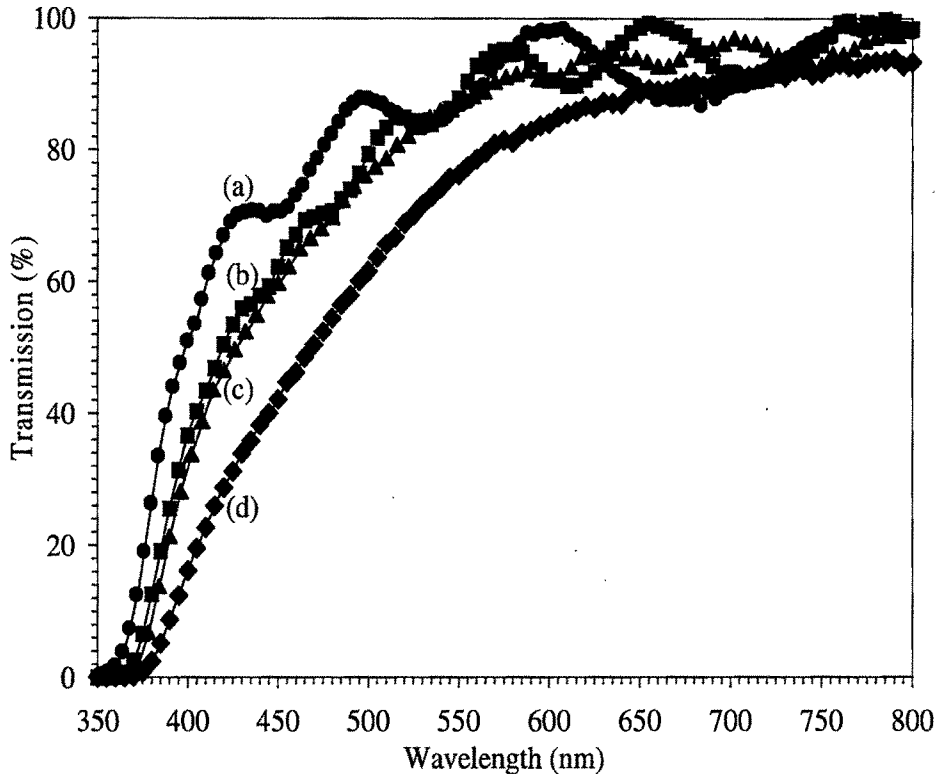


Figure 5.15: The transmission spectra of the AZO thin films deposited at different working pressures: (a) 2 mTorr, (b) 5 mTorr, (c) 10 mTorr, (d) 20 mTorr working pressures.

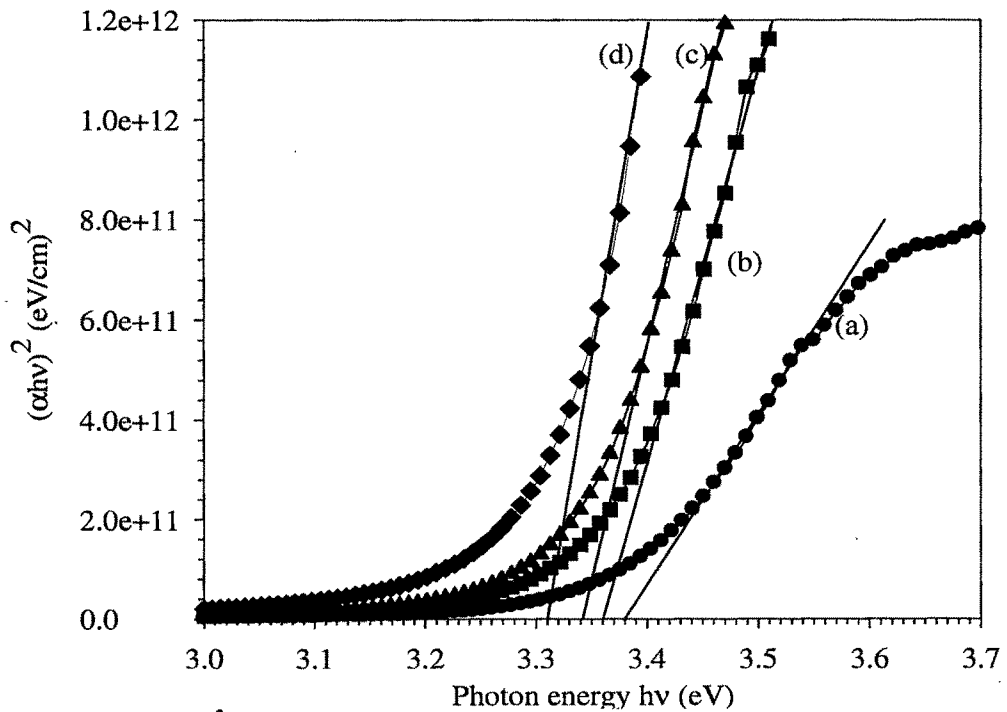


Figure 5.16: Plot of $(\alpha hv)^2$ versus hv for AZO thin films deposited at (a) 2 mTorr, (b) 5 mTorr, (c) 10 mTorr, (d) 20 mTorr working pressures.

5.6.1.4 Electrical Characterization

The sheet resistance and resistivity of AZO thin films grown at different pressures measured using the four-point probe method is shown in table 5.4. It is in the range of 10^{-3} to 10^{-4} Ωcm . At 10 mTorr working pressure, we observed lowest resistivity 6.9×10^{-4} Ωcm . The *n*-type conductivity of as-deposited film is confirmed using the hot-probe method

Table 5.4: The variation in the values of sheet resistance and resistivity of AZO thin films, grown at different working pressure keeping RF power constant at 100W.

Working pressure (mTorr)	Sheet resistance, R_{sh} , (Ω/\square)	Resistivity ρ (Ωcm)
2	50	1.5×10^{-3}
5	37	1.1×10^{-3}
10	23	6.9×10^{-4}
20	29	8.7×10^{-3}

Conclusions

Intrinsic zinc oxide (i-ZnO) and aluminum doped zinc oxide (AZO) thin films are prepared using RF magnetron sputtering technique. i-ZnO films with high resistivity and c-axis orientation structure is deposited at 100 W RF power, keeping deposition pressure constant at 1 mTorr. The as deposited film has dense grain morphology having transmission more than 85 % and energy bandgap of 3.25 eV.

AZO thin films have been obtained by RF-magnetron sputtering by varying the working pressure keeping RF power constant. The structural, optical, electrical, and morphological properties of AZO thin films are analyzed. The obtained films are polycrystalline and have a preferred orientation of the grains with the c-axis perpendicular to the substrates. The lowest resistivity of 6.9×10^{-4} Ωcm is obtained at 100 W RF power and 10 mTorr working pressure. Transmission measurement shows that all films are highly transparent (~85 %) in the visible region. Highly packed uniform grain structure is observed at 100 W RF power and 10 mTorr working pressure.